

Multi-user QKD using quotient graph states derived from continuous-variable dual-rail cluster states

Akash nag Oruganti^{1*}

¹Department of Optics, Palacky University, 17. listopadu 12, Olomouc, 77146, Czech Republic.

Corresponding author(s). E-mail(s): akash.nag.10@gmail.com;

Abstract

Multipartite entangled states are fundamental resources for multi-user quantum cryptographic tasks. Despite significant advancements in generating large-scale continuous-variable (CV) cluster states, particularly the dual-rail cluster state because of its utility in measurement-based quantum computation, its application in quantum cryptography has remained largely unexplored. In this paper, we introduce a novel protocol for generating three user conference keys using a CV dual-rail cluster state. We develop the concept of a quotient graph state by applying a node coloring scheme to the infinite dual-rail graph, resulting in a six-mode pure graph state suitable for cryptographic applications. Our results demonstrate that the proposed protocol achieves performance close to that of GHZ-based protocols for quantum conference key agreement (QCKA), with GHZ states performing slightly better. However, a key advantage of our protocol lies in its ability to generate bipartite keys post-QCKA, a feature not achievable with GHZ states. Additionally, compared to a downstream access network using two-mode squeezed vacuum states, our protocol achieves superior performance in generating bipartite keys. Furthermore, we extend our analysis to the finite-size regime and consider the impact of using impure squeezed states for generating the multipartite entangled states, reflecting experimental imperfections. Our findings indicate that even with finite resources and non-ideal state preparation, the proposed protocol maintains its advantages. We also introduce a more accurate method to estimate the capacity of a protocol to generate bipartite keys in a quantum network.

Keywords: CV-QKD, dual-rail cluster state, conference key agreement, GHZ state, quotient graph state

1 Introduction

Multipartite entangled states are essential resources for various multi-user quantum cryptographic tasks, such as quantum voting [1–3], quantum secret sharing [4–6], multipartite quantum direct communication [7, 8], and quantum conference key agreement (QCKA) [9, 10], among others. These tasks leverage the unique properties of entanglement to enable secure and efficient communication protocols in quantum networks.

In the realm of CV quantum systems, the development and application of multipartite entangled states have predominantly focused on measurement-based quantum computation, particularly using cluster states [11–13]. Despite significant technological advances in the generation of large-scale CV cluster states, especially the dual-rail cluster state, these resources have not been thoroughly explored for quantum cryptographic applications. This gap is notable given the experimental maturity achieved in creating such states through techniques like time [14–17] and frequency domain multiplexing [18–21].

In discrete-variable (DV) systems, Greenberger-Horne-Zeilinger (GHZ) and W states have been identified as ideal resources for QCKA [9, 22]. In CV systems, GHZ and W states are effectively equivalent, both represented by fully symmetric multimode squeezed states [23]. However, it remains uncertain whether these CV equivalents, produced with finite squeezing, are the most suitable multipartite states for QCKA. Unlike DV systems, CV systems offer unique advantages, such as the ability to utilize conditional data post-QCKA to derive additional bipartite keys. This multifaceted use of data enhances the efficiency and security of quantum communication protocols, a feature we explore extensively in this work.

In this paper, we address this gap by introducing a novel protocol for generating a three-user conference key using a CV dual-rail cluster state. To enable its application in QCKA, we introduce the concept of a quotient graph state, employing a node coloring scheme on the infinite dual-rail graph. By forming the quotient graph through vertex identification based on this coloring, we obtain a six-vertex graph representing a pure six-mode graph state. This concept is new and provides a method for state engineering tailored for quantum communication applications, leveraging the properties of the dual-rail cluster state.

We investigate three schemes for generating QCKA in a three-user network:

Direct Reconciliation: The dealer (the one who generates the multipartite state) performs a measurement on one or more modes of the multipartite state, and the outcome is used as the reference to generate the conference key. **Reverse Reconciliation:** One of the remote users' measurements is used as the reference to generate the conference key. **Entanglement-in-the-Middle:** All modes are sent to the remote users without the dealer retaining any part of the state. Any remote user's measurement can serve as the reference, analogous to protocols where entanglement is distributed without a central party. After generating the conference key, the conditional measurement data can still be used to establish bipartite keys post-QCKA between the remaining users. Additionally, we consider generating bipartite keys directly between the dealer and the users without involving QCKA.

Our results demonstrate that the proposed protocol using the dual-rail cluster state and quotient graph state not only outperforms the GHZ/W states generated with the same level of squeezing for QCKA using direct reconciliation, achieving positive key generation under a wider range of channel conditions, but also significantly outperforms them for generating bipartite keys post-QCKA across all methods (direct reconciliation, reverse reconciliation, and entanglement-in-the-middle). Moreover, when compared to a downstream access network utilizing two-mode squeezed vacuum states with equivalent squeezing, our protocol achieves superior performance in generating bipartite keys without involving QCKA.

Recognizing the importance of practical implementations, we extend our analysis to consider real world conditions. We examine the performance of our protocol in the finite-size regime, which is crucial when the number of signals exchanged is limited. Our finite-size analysis provides insights into the key rates achievable under realistic conditions, accounting for statistical fluctuations due to finite sample sizes.

Additionally, we consider the impact of using impure squeezed states for generating the multipartite entangled states. In practical scenarios, experimental imperfections lead to squeezed states that are not perfectly pure [24], affecting the overall performance of quantum protocols. By incorporating impure squeezed states into our analysis, we provide a more realistic assessment of our protocol's robustness against imperfections in state preparation. We find that noisy squeezed states, when trusted and not attributed to eavesdropping, do not adversely affect the security of the protocol and may actually be advantageous. Our findings indicate that the proposed protocol remains effective even with finite resources and non-ideal state preparation.

This study highlights the importance of quotient graph states in CV quantum systems for state engineering in quantum networks, offering improved key rates and robustness against losses, noise, and experimental imperfections. We also introduce a more accurate method for estimating bipartite key rates in downstream access networks, enhancing the evaluation of CV system's key generation capabilities.

This paper is structured as follows: In Section 2, we delve into the complexities of classical information processing for multiple users. Section 3 presents the security analysis of a general multipartite state distributed among trusted users and provides their key rate expressions. In Section 4, we discuss the generation of various tripartite states from squeezed states, including the impact of impurity. In Section 5, we introduce techniques for utilizing dual-rail cluster states in various cryptographic protocols. In section 6 we introduce and analysis various multi-user cryptographic protocols. In section 7 we summarize the major results of our analysis. Finally, in Section 8, we review the outcomes of our research and discuss potential avenues for future work.

2 Multivariate Gaussian Correlations and Multi-User QKD

This section simplifies the discussion of multivariate Gaussian correlations by focusing on three users, A, B, and C, although the principles discussed can be extended to larger networks.

Correlation Scenarios

Symmetric Correlations : All users share equal correlations. Any user can disclose error correction information (syndrome) to enable the others to derive the same raw key, facilitating a shared conference key after privacy amplification.

Centralized Correlations : User A is more strongly correlated with users B and C than they are with each other, allowing for:

- **Conference Key Generation:** User A shares the syndrome, enabling users B and C to establish a conference key.
- **Independent Key Generation:** Users B and C transmit their syndromes to A, allowing A to establish separate keys with each of them.

Induced Correlations : Initially uncorrelated users become correlated if a user or dealer, already correlated with them, shares the necessary syndrome for error correction.

Elaborating on the second and third scenarios, consider three users, specifically A, B and C . A aims to generate a key with B and C , which can be accomplished through two separate techniques. The first technique requires A to convey the essential information for error correction to B and C . Conversely, B and C could forward the necessary information for error correction to A . In the initial scenario, the keys generated will be perfectly correlated as both B and C use the data possessed by A to generate a key. However, in the second scenario, the situation gets more complicated if B and C are correlated, resulting in a potential partial correlation of the keys. In the event of correlations, B and C cannot be treated separately, as the mutual information $I(A : B, C) \neq I(A : B) + I(A : C)$, but rather $I(A : B, C) = I(A : B) + I(A : C|B) = I(A : C) + I(A : B|C)$. The mutual information is defined as $I(i : j) = H(i) - H(i|j) = H(j) - H(j|i)$, and the conditional mutual information $I(i : j|k) = H(i|k) - H(i|j, k)$. $H(\cdot)$ represents the Shannon entropy. When dealing with multiple correlated users, it becomes essential to ascertain the optimal syndrome length, that needs to be transferred for successful error correction. In the given example, B and C must jointly transmit an amount of information quantified as $H(BC|A)$ to A . The restriction lies in the collective syndrome delivered by B and C . The individual syndromes of B , say S_b , and C , say S_c , can exceed in length, provided that $H(S_b, S_c) = H(BC|A)$.

When B and C exhibit no correlation, i.e., $I(B : C) = 0$, this does not necessarily mean that the conditional mutual information $I(B : C|A) = 0$. If both B and C are correlated with A , then disclosing A , or ideally, having A communicate the syndromes to B and C for error correction and to establish a conference key among A, B , and C , will induce a correlation in the conditional data between B and C . This, in turn, enables them to generate a key among themselves. It should be noted that the sequence in which keys are generated influences the nature of the keys that can be produced. In the discussed case, a 1D graph facilitated the creation of a conference key among A, B , and C . Subsequently, B and C are able to establish a key between themselves. Alternatively, if B or C instead of A transmits the syndrome to A , they are capable of creating separate keys with A . In a more general setting, the conditional covariance between B and C , represented as $\langle B_A C_A \rangle = \mathcal{C}_3 - \frac{\mathcal{C}_1 \mathcal{C}_2}{V}$, where B_A and C_A denote the

conditional data held by B and C , disclosing A diminishes the correlation between B and C if $Sgn(\mathcal{C}_1\mathcal{C}_2)/V = Sgn(\mathcal{C}_3)$, eliminates it when $\mathcal{C}_1\mathcal{C}_2/V = \mathcal{C}_3$, and enhances it under other circumstances. Here, $\mathcal{C}_1 = \langle AB \rangle$, $\mathcal{C}_2 = \langle AC \rangle$, $\mathcal{C}_3 = \langle BC \rangle$, and $V = \langle A^2 \rangle = \langle B^2 \rangle = \langle C^2 \rangle$.

3 Security analysis

3.1 Holevo Bound

In the context of CV-QKD, the Holevo bound represents the upper limit on the information accessible to an eavesdropper about the measurement outcomes of the parties whose data are used to generate a secure key. To determine this bound, we assume that the eavesdropper, E , is entangled with all the other parties involved in the protocol, denoted as A , B , and C (we consider three parties for simplicity, but the underlying principles can be extended to more parties and modes). This entanglement leads us to posit that the entire system comprising the eavesdropper and the legitimate parties is in a pure state. Consequently, the von Neumann entropy of the combined system, $S(ABCE)$, is zero. Using the subadditivity property of von Neumann entropy, we obtain the relation $S(E) \leq S(ABC)$ [25]. Similarly, we have $S(E|A) \leq S(BC|A)$. Eve's knowledge of the measurement outcome of A is upper bounded by

$$\chi_A = S(ABC) - S(BC|A).$$

After A generates a key with other correlated parties, B and C share a bipartite state $BC|A$, which could be used to generate a key among them. The Holevo bounds in this case are

$$\chi_{B|A} = S(BC|A) - S(C|BA)$$

and

$$\chi_{C|A} = S(BC|A) - S(B|CA).$$

We consider Gaussian states that are fully described by their first moments (mean quadrature values) and second moments, captured in the covariance matrix Σ . This matrix is defined as:

$$\Sigma_{ij} = \frac{1}{2} \langle \hat{x}_i \hat{x}_j + \hat{x}_j \hat{x}_i \rangle - \langle \hat{x}_i \rangle \langle \hat{x}_j \rangle,$$

where $\langle \cdot \rangle$ denotes expectation values. Diagonal elements of the matrix indicate the variance of each quadrature, representing their uncertainties, while off-diagonal elements represent correlations between different quadratures.

The von Neumann entropy of these states is derived from the symplectic eigenvalues ν_i of the covariance matrix [26] and is given by:

$$S = \sum_i \left[\left(\nu_i + \frac{1}{2} \right) \log \left(\nu_i + \frac{1}{2} \right) - \left(\nu_i - \frac{1}{2} \right) \log \left(\nu_i - \frac{1}{2} \right) \right].$$

Similarly, conditional entropies $S(p|q)$ can be derived from the corresponding conditional covariance matrices. The conditional covariance matrix $\Sigma_{p|q}$ is expressed as:

$$\Sigma_{p|q} = \Sigma_p - \Sigma_{pq}(X\Sigma_qX)^{MP}\Sigma_{pq}^T, \quad (1)$$

where Σ_p denotes the covariance matrix of the unmeasured modes of the multipartite state, Σ_q represents the covariance matrix of the measured modes, Σ_{pq} is the covariance matrix between the measured and unmeasured modes, and X is defined as $Diag(1, 0)$ for measurements in the x-quadrature and MP in Moore-Penrose inverse.

The overall covariance matrix Σ of the system, incorporating both measured and unmeasured modes, is structured as follows:

$$\Sigma = \begin{pmatrix} \Sigma_p & \Sigma_{pq} \\ \Sigma_{pq}^T & \Sigma_q \end{pmatrix} \quad (2)$$

Numerous measurement strategies were explored. We have determined that homodyne measurement of the x-quadrature is the best option for all the multipartite states and protocols presented in this paper. Therefore, any further mention of measurement should be interpreted as homodyne measurement of the x-quadrature.

3.2 Key Rates

Having addressed the complexities of multi-user QKD in the contexts of information reconciliation and the estimation of the Holevo bound, we are now positioned to establish expressions for various key rates. For a three-user system, three distinct types of keys can be generated:

1. Conference Key Agreement (CKA)
2. Bipartite Key Generation post-CKA
3. Independent Bipartite Key Generation

Conference Key Agreement (CKA)

Conference Key Agreement can be realized among the users if there exists at least one user who is correlated with the remaining users. The amount of information (syndrome) that needs to be communicated to the rest of the users is determined by the lowest mutual information between this central user and the other users. The conference key rate can be expressed as:

$$K^i(i : j : k) = \beta \min[I(i : j), I(i : k)] - \chi_i \quad (3)$$

β is the reconciliation efficiency and the superscript signifies the reference data of the user i used to generate the key.

Bipartite Keys Post-CKA

Once the data possessed by user i has been used to generate a conference key, the conditional data possessed by the remaining two users can still be utilized to generate a key between them. The key rate for these scenarios are given by:

$$K^j(j : k|i) = \beta I(j : k|i) - \chi_{j|i} \quad (4)$$

Independent Bipartite Keys

A user can generate independent bipartite keys with the users with whom it is correlated, provided the mutual information of this user (say i) with the rest of the users is higher than the mutual information among the other users (ideally zero). The key rates are:

$$K^j(i : j) = \beta I(i : j) - \chi_j \quad (5)$$

and $K^k(i : k|j)$. In the scenario where the mutual information between the other users is zero, the equation simplifies to $K^k(i : k)$. Notice that even when j and k are identical, the order of key generation influences the key rates. It is more useful to consider the sum of independent keys that i can generate with other users. The actual key rates with each user depend on the information disclosed for error correction, specifically the syndrome length. The sum of independent keys is given by:

$$K^{j,k}(i : jk) = H(j, k) - \zeta H(j, k|i) - \chi_{jk} = K^j(i : j) + K^k(i : k|j) \quad (6)$$

As discussed in Sec. 2, $H(j, k|i)$ represents the optimal amount of information that j and k need to communicate to i to facilitate error correction and $\zeta \geq 1$ accounts for inefficient information reconciliation. For the symmetric case, the independent key rates can be computed as follows:

$$K(i : j) = K(i : k) = \frac{1}{2} [H(j, k) - \zeta H(\mathbf{S}_j, \mathbf{S}_k) - S(ijk) + S(i | jk)] \quad (7)$$

Here, \mathbf{S}_j and \mathbf{S}_k are the syndromes with entropies $H(\mathbf{S}_j) = H(\mathbf{S}_k)$. In this article, we focus on the conditions under which a positive key rate can be achieved, and therefore, we emphasize the sum of independent keys rather than individual key rates.

3.3 Finite Size Analysis

In practical implementations, the number of exchanged quantum signals is inherently finite. This finite data sample introduces statistical fluctuations that can significantly impact the security and performance of the QKD protocol. Unlike the asymptotic regime, discussed in the previous section, where it is assumed that an infinite number of signals are exchanged, allowing statistical uncertainties to vanish. In the finite-size regime, the key rate is affected by the statistical estimation of channel parameters.

The order in which error correction and parameter estimation are performed affects the finite-size key rate expression [27]. When error correction is performed *after* parameter estimation, some transmitted signals are disclosed to estimate the channel parameters. Let N be the total number of signals exchanged, and n be the number of signals used for key generation after discarding $N - n$ signals for parameter estimation. The finite-size key rate K is given by:

$$K = \frac{n}{N} [K_\infty(t^{\text{low}}, V_\epsilon^{\text{up}}) - \Delta(n)] \quad (8)$$

Alternatively, when error correction is performed *before* parameter estimation, all measurements can be used for both parameter estimation and key generation, allowing

for better estimates of the channel parameters since no data is discarded. In this case, the finite-size key rate K is:

$$K = K_\infty(t^{\text{low}}, V_\epsilon^{\text{up}}) - \Delta(n) \quad (9)$$

In both expressions, $K_\infty(t^{\text{low}}, \epsilon_{\text{up}})$ is the asymptotic key rate calculated using conservative estimates of the channel transmission t and excess noise $V_\epsilon = t\epsilon$ to account for statistical fluctuations due to the finite sample size. These adjusted parameters are:

$$\tau^{\text{low}} = \tau - 6.5 \sigma_t \quad (10)$$

$$V_\epsilon^{\text{up}} = V_\epsilon + 6.5 \sigma_\epsilon \quad (11)$$

where σ_t and σ_ϵ are the standard deviations of the estimators of t and V_ϵ , respectively (see Appendix C). The factor 6.5 corresponds to a confidence level ensuring an error probability of 10^{-10} . The finite-size correction term $\Delta(n)$ [28] accounts for the statistical fluctuations in the mutual information:

$$\Delta(n) = 7 \sqrt{\frac{\log_2(2 \times 10^{10})}{n}} \quad (12)$$

with n being the number of signals used for key generation.

4 Generation of Tripartite States

The generation of multipartite states in CV systems can be efficiently realized by manipulating squeezed light states through beam splitters [29, 30]. This method allows us to explore different configurations of squeezed states and beam splitters that result in distinct tripartite states. We define a general structure of the covariance matrix as follows:

$$\begin{pmatrix} V_A & C_{AB} & C_{AC} \\ C_{AB} & V_B & C_{BC} \\ C_{AC} & C_{BC} & V_C \end{pmatrix} \quad (13)$$

Here, V_i represents the variance of mode $i = A, B, C$, and C_{ij} denotes the covariance between the quadratures of modes i and j .

We consider two configurations: the symmetric GHZ-like state and the downstream access network (DAN). The GHZ-like state is of interest because it has maximum correlation equally distributed among all modes, The DAN configuration is appealing because it can be easily implemented by substituting the two-mode squeezed vacuum with either modulated squeezed or coherent states, and it offers an advantage in producing bipartite keys.

In the first configuration, referred to as the **Symmetric GHZ-like state**, three squeezed states with x -quadrature variances $V_1 = V$, $V_2 = \frac{1}{V}$, and $V_3 = \frac{1}{V}$ are directed into two beam splitters with transmissions $t_1 = \frac{2}{3}$ and $t_2 = \frac{1}{2}$ (see Fig. 1). This setup yields a symmetric covariance matrix where

$$V_A = V_B = V_C = \text{Diag} \left[\frac{1 + 2V^2}{3V}, \frac{2 + V^2}{3V} \right],$$

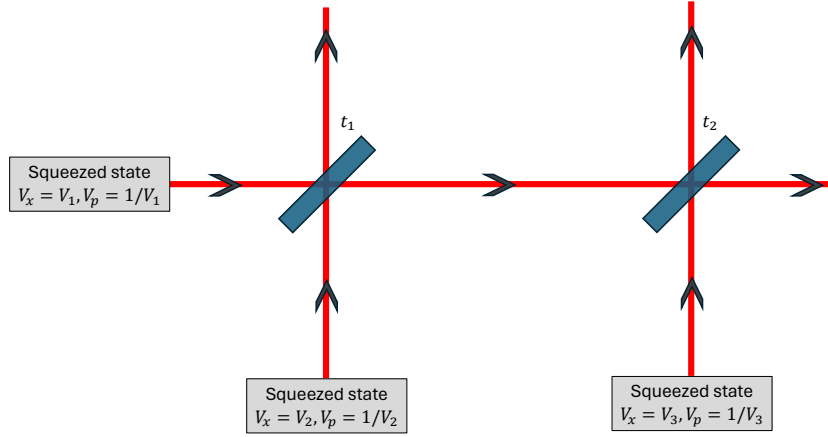


Fig. 1: Schematic diagram for generating tripartite states

and the covariances between modes are given by

$$C_{AB} = -C_{AC} = C_{BC} = \text{Diag} \left[\frac{V^2 - 1}{3V}, \frac{1 - V^2}{3V} \right].$$

This state exhibits maximum correlation equally among all modes, analogous to the GHZ state in discrete-variable systems.

The second configuration is based on the **Downstream Access Network (DAN)** approach, which is a cost-effective setup for generating tripartite states. In this scheme, two squeezed states with x -quadrature variances $V_1 = V$ and $V_2 = \frac{1}{V}$, along with a vacuum mode $V_3 = 1$, are combined using two beam splitters, with transmissions $t_1 = t_2 = \frac{1}{2}$. This results in a covariance matrix where

$$V_A = \text{Diag} \left[\frac{1 + V^2}{2V}, \frac{1 + V^2}{2V} \right], \quad V_B = V_C = \text{Diag} \left[\frac{(1 + V)^2}{4V}, \frac{(1 + V)^2}{4V} \right],$$

$$C_{AB} = -C_{AC} = \text{Diag} \left[\frac{V^2 - 1}{2\sqrt{2}V}, \frac{1 - V^2}{2\sqrt{2}V} \right], \quad C_{BC} = \text{Diag} \left[-\frac{(V - 1)^2}{4V}, -\frac{(1 - V)^2}{4V} \right].$$

This configuration simplifies implementation and reduces costs compared to other schemes, as the two-mode squeezed vacuum can be replaced with a modulated squeezed state.

4.0.1 Effect of Impurity in Squeezed States

In practical implementations, squeezed states are often not pure due to technical imperfections and decoherence, which introduce additional noise in the anti-squeezed

quadrature, which usually is proportional to the degree of squeezing [24]. We characterize this impurity by an additional noise parameter V_N , such that if the variance of the squeezed quadrature is V , the variance of the anti-squeezed quadrature becomes $V_N + 1/V$.

To account for the impurity, we modify the covariance matrices of the input squeezed states. For the GHZ-like state configuration, the covariance matrices of the input squeezed states become

$$V_1 = \text{Diag} \left[V, V_N + \frac{1}{V} \right], \quad V_2 = V_3 = \text{Diag} \left[V_N + \frac{1}{V}, +V \right].$$

Similarly, for the DAN configuration, the covariance matrices are

$$V_1 = \text{Diag} \left[V, V_N + \frac{1}{V} \right], \quad V_2 = \text{Diag} \left[V_N + \frac{1}{V}, V \right], \quad V_3 = \text{Diag} [1, 1].$$

Using these modified input variances, we can compute the resulting covariance matrices after the beam splitter transformations, taking into account the impurity.

For the **GHZ-like state** with impure squeezed states, the variances and covariances become

$$V_A = V_B = V_C = \text{Diag} \left[\frac{1 + 2V^2 + VV_N}{3V}, \frac{2 + V^2 + 2VV_N}{3V} \right],$$

and the covariances between modes are given by

$$C_{AB} = -C_{AC} = C_{BC} = \text{Diag} \left[\frac{V^2 - 1 - VV_N}{3V}, \frac{1 - V^2 + VV_N}{3V} \right].$$

For the **DAN** configuration, the variances and covariances are

$$\begin{aligned} V_A &= \text{Diag} \left[\frac{1 + V^2 + VV_N}{2V}, \frac{1 + V^2 + VV_N}{2V} \right], \\ V_B = V_C &= \text{Diag} \left[\frac{(1 + V)^2 + VV_N}{4V}, \frac{(1 + V)^2 + VV_N}{4V} \right], \\ C_{AB} = -C_{AC} &= \text{Diag} \left[\frac{V^2 - 1 - VV_N}{2\sqrt{2}V}, \frac{1 - V^2 + VV_N}{2\sqrt{2}V} \right], \\ C_{BC} &= \text{Diag} \left[-\frac{(V - 1)^2 + VV_N}{4V}, -\frac{(1 - V)^2 + VV_N}{4V} \right]. \end{aligned}$$

By incorporating the impurity parameter V_N , we can examine the effect of non-ideal squeezing on the generated tripartite states. The presence of additional noise increases the variances of the anti-squeezed quadratures, thereby impacting the correlations among the modes. This noise must be carefully accounted for to ensure the viability of cryptographic tasks. We assume that this preparation noise is trusted and does not provide information to eavesdroppers.

To address this, we introduce an additional mode for each squeezed state to account for the noise, ensuring that the two modes together form a pure bipartite state. Specifically, we consider the impure squeezed state as one of the outputs of a beam splitter fed by two pure squeezed states with x-quadrature variances Γ_1 and Γ_2 at the input. The impure squeezed state are then related to the variances of the input pure squeezed states as follows:

$$\Gamma_1 = V - \frac{V^3 V_N}{\sqrt{V^3 V_N (1 + V^3 V_N)}}, \quad \Gamma_2 = V + \frac{V^3 V_N}{\sqrt{V^3 V_N (1 + V^3 V_N)}}. \quad (14)$$

5 Dual-rail cluster state for QKD

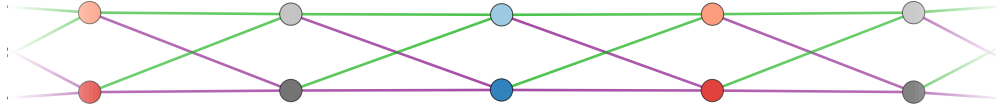
In this analysis, we propose a distribution strategy for the modes of a dual-rail cluster state in a multi-node QKD network. Unlike a finite graph defined by a discrete set of nodes, the dual-rail cluster state represents an open-ended, repeating lattice of interconnected modes. Each mode is typically linked to four others, creating an extensive and complex structure that is difficult to handle as is.

To make this infinitely repeating configuration more tractable, we introduce a coloring scheme inspired by graph theory terminology. By assigning colors to modes and then grouping all modes of the same color together, we form what we call a quotient graph state. This quotient graph serves as a finite, homomorphic image of the original dual-rail lattice, preserving key connectivity patterns while reducing its complexity. Although we draw on terms like “coloring” and “quotient graph” from graph theory, our approach focuses on using these concepts to describe and manage the grouping process, rather than relying on advanced graph-theoretic techniques.

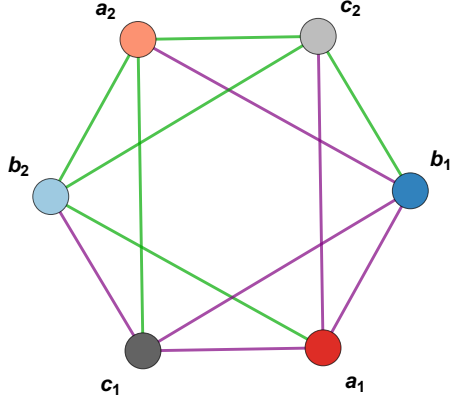
The resulting quotient graph state provides a simplified framework that retains the essential structural features of the dual-rail cluster state. In doing so, it creates a more manageable platform for implementing robust and scalable continuous-variable QKD protocols, ensuring that the underlying entanglement resources can be effectively harnessed in practical quantum communication networks.

The optimal homomorphic graph corresponds to a six-mode graph state, achievable through a coloring strategy detailed in Fig. 2. The covariance matrix of this six-mode graph state is (refer to Sec: A for derivation):

$$\begin{pmatrix} V & 0 & C & -C & C & C \\ 0 & V & C & -C & -C & -C \\ C & C & V & 0 & C & -C \\ -C & -C & 0 & V & C & -C \\ C & -C & C & C & V & 0 \\ C & -C & -C & -C & 0 & V \end{pmatrix} \quad (15)$$



(a) Dual rail cluster state



(b) 6 mode graph state

Fig. 2: (a) Shows the coloring scheme of dual rail cluster state to obtain the six mode graph state (c). The edges in the graph illustrates the correlations between modes, with edges in two colors indicating the sign of the correlation. Edges of one color represent positive correlations, while edges of the other color represent negative correlations.

where the diagonal covariance matrix \mathbf{V} and the off-diagonal covariance matrix \mathbf{C} are defined as follows for pure squeezed states:

$$\mathbf{V} = \begin{pmatrix} \frac{1+V^2}{2V} & 0 \\ 0 & \frac{1+V^2}{2V} \end{pmatrix}, \quad \mathbf{C} = \begin{pmatrix} \frac{1-V^2}{4V} & 0 \\ 0 & \frac{V^2-1}{4V} \end{pmatrix}. \quad (16)$$

V is the variance of the squeezed quadrature of the squeezed state. For impure squeezed states, as described in the previous section, the impurity parameter V_N modifies these matrices to:

$$\mathbf{V} = \begin{pmatrix} \frac{1+V^2+V_N}{2V} & 0 \\ 0 & \frac{1+V^2+V_N}{2V} \end{pmatrix}, \quad \mathbf{C} = \begin{pmatrix} \frac{1-V^2+VV_N}{4V} & 0 \\ 0 & \frac{V^2-1-VV_N}{4V} \end{pmatrix}. \quad (17)$$

This six-mode graph state provides a versatile platform for various QKD strategies. We present optimal methods for generating a three-user conference key and independent bipartite keys, which we compare to the three-mode tripartite states discussed in the previous section.

5.1 Distribution strategies for six-mode graph state

We identify four primary strategies for distributing quantum states among users, depending on whether the dealer also serves as one of the users or acts solely as a distributor.

Dealer as a Participant

1. **Distribution 1 (Fig.3a)**: The dealer sends mode b_1 and mode c_1 to two distant users through a channel characterized by channel transmission t and channel excess noise ϵ transforming the modes to \tilde{b}_1 and \tilde{c}_1 , with covariance matrix $\tilde{V} = t(\mathbf{V} + \epsilon\mathbb{I} - \mathbb{I}) + \mathbb{I}$, \mathbb{I} here is 2×2 identity matrix. The dealer retains the rest of the modes, a_1, a_2, b_2 , and c_2 .
2. **Distribution 2 (Fig.3b)**: The dealer sends modes b_1 and b_2 to one user and modes c_1 and c_2 to the other user. The dealer retains modes a_1 and a_2 .

Dealer as a Distributor

1. **Distribution 3 (Fig.3c)**: Modes a_1, b_1 , and c_1 are distributed to three separate users, the rest are retained by the dealer.
2. **Distribution 4 (Fig.3d)**: All the modes are sent through the channel to three remote users, one user gets a_1 and a_2 , another receives b_1 and b_2 , and the third c_1 and c_2 .

Each of these strategies offers distinct advantages, and the choice of strategy should consider the operational context and security requirements of the QKD system.

6 Quantum conference key distribution protocols

Quantum conference key distribution protocols like standard two user QKD protocols can be broadly categorized into three categories, based on the role of the dealer and the method of key reconciliation. Understanding these protocols is essential for evaluating the security and efficiency of multi-user quantum communication systems. In our analysis, we assume that the channel parameters are symmetric, meaning that all users have identical channel conditions.

Direct Reconciliation (DR)

In the direct reconciliation protocol, the dealer retains one or more modes of the multipartite state they prepare and uses their measurement outcomes as references for key generation. The remote parties receive the necessary information and perform the required error correction.

For the GHZ state described in Sec.4, the covariance matrix given in Eq.13 transforms to:

$$\begin{pmatrix} V_A & \sqrt{t}C_{AB} & \sqrt{t}C_{AC} \\ \sqrt{t}C_{AB} & t(V_B + \epsilon - 1) + 1 & tC_{BC} \\ \sqrt{t}C_{AC} & tC_{BC} & t(V_C + \epsilon - 1) + 1 \end{pmatrix} \quad (18)$$

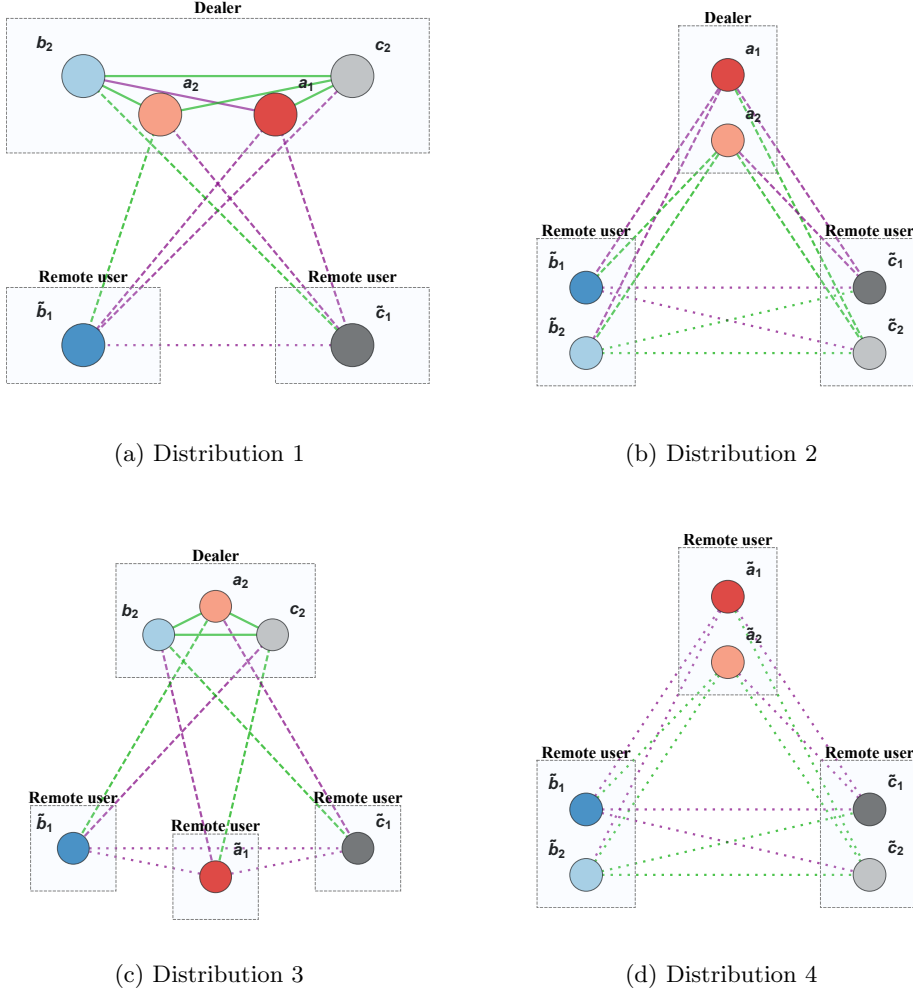


Fig. 3: The graphs depict various methods for distributing a six-mode graph state among three users. Dashed lines indicate that the correlations (i.e., covariance between the modes C) have been reduced by a factor of \sqrt{t} , while dotted lines indicate a reduction by a factor of t .

The key rate for this approach is given by $k^A(A : \tilde{B} : \tilde{C})$ (refer to Eq. 3), where the notation \tilde{i} indicates that mode i has been transmitted through a quantum channel.

We explore two distribution strategies for a six-mode graph state intended for three-user conference key generation via direct reconciliation, as illustrated in Figs. 3a and 3b.

There are multiple methods for conference key generation based on *Distribution 1* (Fig. 3a). Among these, the key $k^{a_1}(a_1 : \tilde{b}_1 : \tilde{c}_1 | a_2)$ proves most robust against channel losses and noise in the asymptotic regime when reconciliation efficiency is

perfect ($\beta = 1$); see Fig.4a. Note that a_1 and a_2 are not interchangeable due to the correlation type (sign) with the remote user's modes. Depending on the channel parameters, leveraging measurements from multiple modes as references can further enhance the conference key rate.

From Fig.4a, we observe that under finite squeezing, the GHZ state is not the optimal multipartite resource for maximizing distance in conference key generation with direct reconciliation under ideal conditions. Among the configurations tested, *Distribution 1* achieves the greatest distances, particularly under high excess channel noise ($0.08 < \epsilon < 0.5$ SNU). Although trusted noise does not hinder the performance of *Distribution 1* or GHZ-based protocols in the asymptotic regime (and may even assist them), it offers no similar advantage to *Distribution 2*, yet it does not significantly degrade its performance either.

In the finite-size regime, for $n = 10^7$ measurements and imperfect reconciliation ($\beta = 0.95$), *Distribution 2* (Fig.3b) with key rate $k^{a_1}(a_1 : \tilde{b}_1\tilde{b}_2 : \tilde{c}_1\tilde{c}_2 | a_2)$ enables key generation over greater distances for channel noise $0 < \epsilon < 0.27$ SNU; see Fig. 5a. This is in contrast of what we observe in asymptotic regime where *Distribution 1* enables key generation for the largest distances. This is due to the fact that *Distribution 2* enables the users and the dealer to use four correlations as opposed to three for *Distribution 1* to enable better estimation of the channel parameters (see Sec. C).

Reverse Reconciliation (RR)

Contrary to direct reconciliation, reverse reconciliation involves a remote user serving as the reference. This user sends error correction information to the dealer and other participants, facilitating key alignment based on their reference measurements.

The conference key rate for tripartite states under reverse reconciliation is given by $k^{\tilde{B}}(A : \tilde{B} : \tilde{C})$.

For the six-mode graph state with *Distribution 1* (Fig.3a), we find that the optimal key rate for achieving higher tolerance to channel parameters under reverse reconciliation is

$$k^{\tilde{b}_1}(a_1 : \tilde{b}_1 : \tilde{c}_1 | b_2 a_2 c_2).$$

For *Distribution 2* (Fig. 3b), the optimal conference key is

$$k^{\tilde{b}_1}(a_1 a_2 : \tilde{b}_1 \tilde{b}_2 : \tilde{c}_1 \tilde{c}_2 | \tilde{b}_2).$$

From Fig.4b, it is apparent that the GHZ state generates positive keys under a broader range of channel conditions. Comparable performance is achieved with *Distribution 1*. The influence of trusted noise for reverse reconciliation is the same as for direct reconciliation, it shows little to no effects on protocols with *Distribution 2* but benefits protocols with *Distribution 1* and the GHZ state.

In the finite size regime; see Fig. 5b, the trend remains the same, with the GHZ state enabling the largest distances followed by *Distribution 1* and *Distribution 2*. Though the difference is not significant.

Entanglement in the middle (Mid)

In this protocol, the dealer prepares entangled states and distributes them among the users but does not have access to the conference key being generated.

The conference key rate for tripartite states in the entanglement-in-the-middle protocol is given by $k^{\tilde{A}}(\tilde{A} : \tilde{B} : \tilde{C})$.

For the six-mode graph state with *Distribution 3* (Fig.3c), the dealer discloses the measurement outcomes of all of their modes, effectively disconnecting themselves from the conditional data held by the other users. This leads to the conference key rate between the users being

$$k^{\tilde{a}_1}(\tilde{a}_1 : \tilde{b}_1 : \tilde{c}_1 | a_2 b_2 c_2).$$

It should be noted that instead of disclosing the measurement outcomes, the dealer can generate three sets of conference keys with any two remote users, with conference key rates $k^{a_2}(a_2 : \tilde{b}_1 : \tilde{c}_1)$, $k^{b_2}(b_2 : \tilde{a}_1 : \tilde{c}_1 | a_2)$, and $k^{c_2}(c_2 : \tilde{a}_1 : \tilde{b}_1 | a_2 b_2)$. However, the tolerance to channel noise and loss for the conference key $k^{b_2}(b_2 : \tilde{a}_1 : \tilde{c}_1 | a_2)$ was found to be very low.

For the *Distribution 4* (Fig.3b), the optimal conference key is

$$k^{\tilde{a}_1 \tilde{a}_2}(\tilde{a}_1 \tilde{a}_2 : \tilde{b}_1 \tilde{b}_2 : \tilde{c}_1 \tilde{c}_2).$$

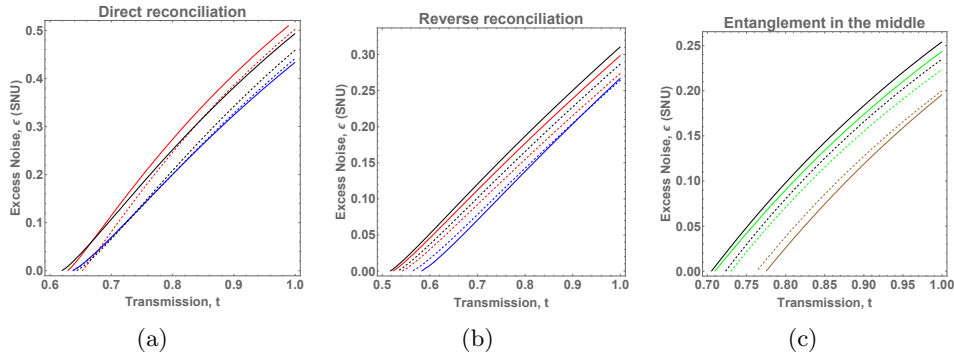


Fig. 4: These plots illustrate the maximum tolerable channel losses and noise in asymptotic regime, key generation is possible only for channel parameters lying below the plotted curves. The blue curve corresponds to *Distribution 2*, the red to *Distribution 1*, the green to *Distribution 3*, the brown to *Distribution 4*, and the black to the GHZ state. Dashed lines represent pure squeezed states, while solid lines indicate impure but trusted squeezed states with $\Delta V = 10$. The reconciliation efficiency is $\beta = 1$, and the variance of the squeezed quadrature is $V = 0.1$ SNU.

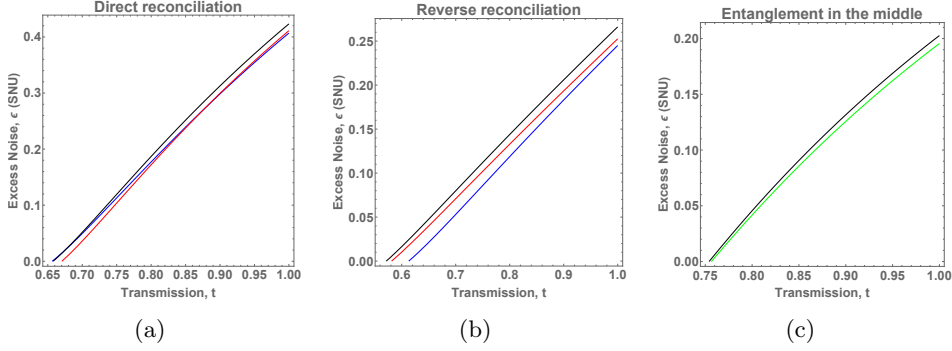


Fig. 5: These plots illustrate the maximum tolerable channel losses and noise in finite size regime with $n = 10^7$ measurements, key generation is possible only for channel parameters lying below the plotted curves. The blue curve corresponds to *Distribution 2*, the red to *Distribution 1*, the green to *Distribution 3*, and the black to the GHZ state. With trusted AS noise $\Delta V = 10SNU$. The reconciliation efficiency is $\beta = 0.95$, and the variance of the squeezed quadrature is $V = 0.1SNU$.

From Fig.4c, we observe that, similar to the case in reverse reconciliation, the protocol with the GHZ state outperforms other protocols. *Distribution 3* closely matches the GHZ state’s performance. The adverse influence of trusted noise for *Distribution 4* is noticeable here, though its presence proves beneficial for protocols with *Distribution 3* and the GHZ state.

In contrast to *Distribution 3*, neither the GHZ state nor *Distribution 4* can directly estimate the channel transmission between the dealer and the users. To enable channel parameter estimation, the dealer must occasionally retain, measure, and disclose a subset of the modes. In Fig.5c, we allocate half of the 10^7 measurements for channel estimation and use the remaining half for key generation. Under these conditions, while the GHZ state still maintains a slight advantage, the performance gap narrows considerably.

Bipartite key post CKA

Following the generation of a conference key using any of the schemes mentioned in the previous section, bipartite keys can be generated using the conditional data of the remaining users. This data, conditioned on the reference data used for conference key generation, allows for the creation of additional bipartite keys. The following table (Tab.1) summarizes various scenarios and their corresponding key rate expressions.

Scenario	Tripartite-States Key Rate	Distribution	Key Rate
Bipartite key rate post CKA with DR	$k^{\tilde{B}}(\tilde{B} : \tilde{C} A)$	<i>Distribution 1</i> <i>Distribution 2</i>	$k^{\tilde{b}_1}(\tilde{b}_1 : \tilde{c}_1 a_1 a_2)$ $k^{\tilde{b}_1 \tilde{b}_2}(\tilde{b}_1 \tilde{b}_2 : \tilde{c}_1 \tilde{c}_2 a_1 a_2)$
Bipartite key rate with DR post CKA with RR	$k^A(A : \tilde{C} \tilde{B})$	<i>Distribution 1</i> <i>Distribution 2</i>	$k^{a_1}(a_1 : \tilde{c}_1 b_2 a_2 c_2 \tilde{b}_1)$ $k^{a_1 a_2}(a_1 a_2 : \tilde{c}_1 \tilde{c}_2 \tilde{b}_1 \tilde{b}_2)$
Bipartite key rate with RR post CKA with RR	$k^{\tilde{C}}(A : \tilde{C} \tilde{B})$	<i>Distribution 1</i> <i>Distribution 2</i>	$k^{\tilde{c}_1}(a_1 : \tilde{c}_1 b_2 a_2 c_2 \tilde{b}_1)$ $k^{\tilde{c}_1 \tilde{c}_2}(a_1 a_2 : \tilde{c}_1 \tilde{c}_2 \tilde{b}_1 \tilde{b}_2)$
Bipartite key rate post CKA with Mid	$k^{\tilde{B}}(\tilde{B} : \tilde{C} \tilde{A})$	<i>Distribution 3</i> <i>Distribution 4</i>	$k^{\tilde{b}_1}(\tilde{b}_1 : \tilde{c}_1 a_2 b_2 c_2 \tilde{a}_1)$ $k^{\tilde{b}_1 \tilde{b}_2}(\tilde{b}_1 \tilde{b}_2 : \tilde{c}_1 \tilde{c}_2 \tilde{a}_1 \tilde{a}_2)$

Table 1: Summary of bipartite key rates post QCKA for different scenarios and distributions

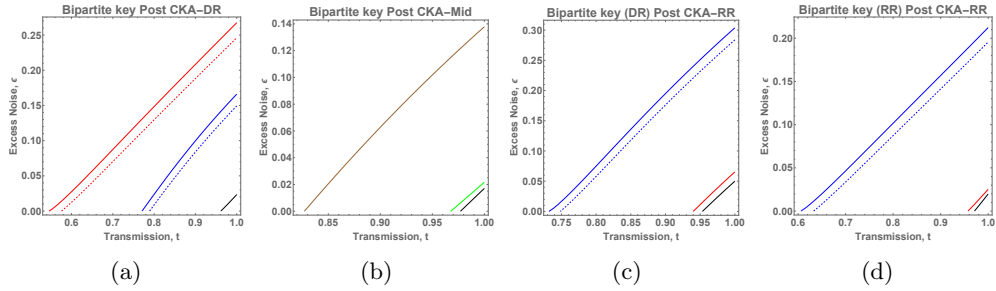


Fig. 6: Maximum tolerable excess noise ϵ (in SNU) for varying transmission of the channel t for generation of bipartite keys post CKA generation. The blue curve corresponds to *Distribution 2*, the red to *Distribution 1*, the green to *Distribution 3*, the brown to *Distribution 4*, and the black to the GHZ state. Dashed lines corresponds to finite size keys, while solid lines corresponds to asymptotic keys. For AS noise of $\Delta V = 10$, the reconciliation efficiency is $\beta = 0.95$, and the variance of the squeezed quadrature is $V = 0.1$ SNU.

When comparing the overall multiuser quantum key distribution (QKD) capabilities (CKA and subsequent bipartite key generation) of multipartite states, the six-mode graph state derived from a dual rail cluster state significantly outshines the GHZ state: see Fig.6. For CKA via DR, *Distribution 1* supports CKA and bipartite key generation under a broader range of channel conditions than any other considered multipartite state or strategy. For CKA via RR, *Distribution 2* excels beyond all others. For CKA via Mid, *Distribution 4* facilitates CKA and bipartite keys under more extensive channel conditions. In the finite-size regime, bipartite keys generated using the GHZ state become infeasible for measurements with fewer than $n = 10^8$ samples. In contrast, protocols employing dual-rail cluster states enable the generation of bipartite keys after the conference key is established, making them applicable

to all the protocols introduced. However, the distribution strategy must be carefully tailored to the specific requirements of the quantum network.

Independent bipartite keys

In Sec.3, we discussed the utility of analyzing the sum of independent bipartite keys that can be generated by a central user who has higher correlations with other users. This approach is particularly informative in symmetric cases, where the collective key rate helps establish bounds on the symmetric channel parameters required for independent key generation by all the users with the central user. As outlined in Sec. 2, generating independent keys necessitates one user having a stronger correlation with the rest of the users than between the users themselves.

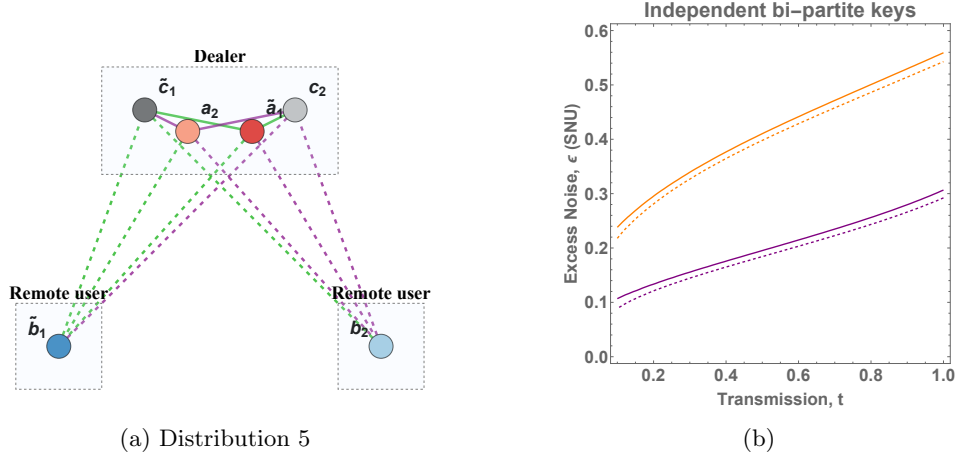


Fig. 7: b) Shows maximum tolerable excess noise ϵ for varying transmission of the channel t for generating independent bipartite keys between the dealer and the remote users. Brown plots correspond to Distribution 5 (a) and the purple plot corresponds to DAN. Dashed line corresponds to finite size keys ($n = 10^7$) and solid lines corresponds to asymptotic keys. For AS noise of $\Delta V = 10$, the reconciliation efficiency is $\beta = 0.95$, and the variance of the squeezed quadrature is $V = 0.1$ SNU.

It is more advantageous in terms of classical information processing for these remote users to be uncorrelated. We introduce a *Distribution 5*, depicted in Fig.7a, specifically because the remote users are not correlated. It is evident from Fig.7b that this approach offers a significant enhancement compared to DAN.

7 Results

In this work, we introduced a novel protocol for three-user conference key generation using dual-rail cluster states, employing the concept of a **quotient graph state** to

create a finite six-mode pure graph state suitable for cryptographic applications. Our comparative analysis with GHZ/W states generated under similar squeezing conditions yielded the following key findings:

- **Asymptotic Regime (CKA):** In the limit of infinite signals, our protocol outperforms GHZ/W states in the direct reconciliation scheme but does not surpass them in reverse reconciliation or entanglement-in-the-middle schemes.
- **Finite-Size Regime (CKA):** GHZ states maintain a slight performance advantage for generation of conference key in all schemes explored, direct reconciliation, reverse reconciliation, and entanglement-in-the-middle. However, the performance gap narrows significantly as our protocol leverages multiple modes per user, enhancing channel parameter estimation and mitigating finite-size effects. This improvement brings the key rates closer to those achieved with GHZ states, reducing the impact of statistical fluctuations inherent in finite-size scenarios.
- **Bipartite Key Generation Post-QCKA:** Our protocol significantly outperforms GHZ states in generating bipartite keys after the conference key agreement across all methods (direct reconciliation, reverse reconciliation, and entanglement-in-the-middle). The ability to derive additional bipartite keys post-QCKA enhances the overall efficiency and security of the quantum network.
- **Bipartite Key Generation Without QCKA:** When compared to downstream access networks utilizing two-mode squeezed vacuum states with equivalent squeezing, our protocol achieves superior performance in generating bipartite keys without involving QCKA. This demonstrates the versatility of our protocol in supporting both conference and individual key generation within the network.
- **Robustness to Imperfections:** The protocol maintains its advantages even when using impure squeezed states (provided the impurity is trusted), demonstrating robustness against experimental imperfections. This robustness is critical for practical implementations where perfect state preparation is challenging.

8 Conclusion

In this work, we have introduced a novel protocol for three-user conference key generation using dual-rail cluster states, employing the concept of a *quotient graph state* to create a six-mode pure graph state suitable for cryptographic applications. Our comparative analysis with GHZ/W states generated under similar squeezing conditions has yielded significant insights.

In the asymptotic regime, where the number of signals approaches infinity, our protocol outperforms GHZ/W states in the direct reconciliation scheme but does not surpass them in reverse reconciliation or entanglement-in-the-middle schemes. In the finite-size regime, GHZ states still perform marginally better in each scheme. However, the performance gap narrows significantly as our protocol benefits from each user accessing multiple modes, which enhances channel parameter estimation and mitigates finite-size effects. This improved estimation reduces the impact of statistical fluctuations, bringing the maximum achievable distances closer to those achieved with GHZ states.

Additionally, our protocol significantly outperforms GHZ/W states in generating bipartite keys after the conference key agreement across all methods. It also surpasses downstream access networks utilizing two-mode squeezed vacuum states in generating bipartite keys without involving QCKA. This versatility demonstrates the adaptability of our protocol in supporting both conference and individual secure communications within the network.

Our protocol maintains its advantages even when using impure squeezed states, showcasing robustness against experimental imperfections. This robustness is critical for practical implementations where perfect state preparation is challenging.

These results underscore the importance of tailoring quantum cryptographic solutions to the specific demands of quantum networks. The use of dual-rail cluster states and quotient graph states provides a pathway to more robust, flexible, and efficient quantum cryptographic protocols with continuous-variable systems.

Looking ahead, the insights gained from this work highlight several promising directions for future research. Exploring alternative multipartite states with configurations that allow users to access multiple modes could further enhance key rates and robustness in quantum communication protocols. Extending the protocol to networks with more than three users and examining the performance benefits in larger, more complex quantum networks is a natural progression. Developing advanced methods for channel parameter estimation that leverage access to multiple modes per user could further mitigate finite-size effects and improve the security and efficiency of the protocols. Pursuing experimental validation of the proposed protocol, including the generation of quotient graph states and testing under realistic conditions with impure squeezed states, would bridge the gap between theory and practice. Additionally, extending the security analysis to consider more sophisticated eavesdropping strategies would verify the protocol's robustness against a wider range of attacks.

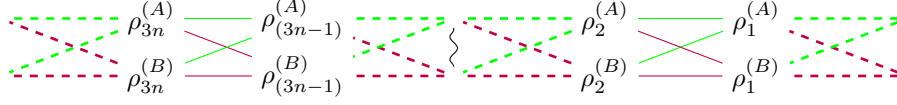
Acknowledgements

I would like to acknowledge Vladyslav Usenko, Ivan Derkach, Tobias Gehring, Christoph Pacher, Florian Kanitschar, and Ulrik Lund Andersen for their valuable discussions. A. O. acknowledge the project 8C22002 (CVStar), which have received funding from the European Union's Horizon 2020 research and innovation framework programme under grant agreement No. 731473 and 101017733, and the project No. 21-44815L of the Czech Science Foundation. A. O. acknowledges the project IGA-PrF-2024-008 of Palacky University Olomouc.

Appendix A Dual rail cluster state to six mode graph state

In Sec.5, we introduced a method to generate a pure six-mode graph state from a dual-rail cluster state. Here, we provide a justification for this method. Since we are working with Gaussian states, it suffices to show that, after appropriately grouping the nodes as suggested by the coloring scheme in Fig.2a, the covariance matrix of the resulting state corresponds to that of a pure six-mode graph state.

The dual-rail cluster state, denoted here by ρ_{dual} , consists of two parallel chains (rails) of quantum states: Rail A and Rail B . Each node (quantum state) in these rails is uniquely identified by its rail (A or B) and its position i along that rail as illustrated bellow.



To construct the six-mode graph state, we group the nodes from each rail into three groups by selecting every third node. For each node at position i in rail R , we define the constituent state $\rho_i^{(R)}$ as the reduced density operator obtained by tracing out all other nodes from the dual-rail cluster state ρ_{dual} :

$$\rho_i^{(R)} = \text{Tr}_i^{(R)} (\rho_{\text{dual}}),$$

where $\text{Tr}_i^{(R)}$ denotes the partial trace over all modes except the one at position i in rail R . We then form statistical mixtures by averaging the constituent states within each group. For each group $j \in \{1, 2, 3\}$ in rail R , the mixed state $\rho_j^{(R)}$ is defined as:

$$\rho_j^{(R)} = \frac{1}{n} \sum_{m=1}^n \rho_{3m-(3-j)}^{(R)}, \quad (\text{A1})$$

where n is the total number of grouping repetitions along each rail. Specifically, the positions i of the nodes included in each group are:

- For $j = 1$: positions $i = 3m - 2$,
- For $j = 2$: positions $i = 3m - 1$,
- For $j = 3$: positions $i = 3m$,

with $m \in \{1, 2, \dots, n\}$.

By forming these statistical mixtures, we create six mixed states in total (three groups in each of the two rails). The quadrature operators associated with these mixed states are denoted $\mathbf{x}_j^{(R)}$ and $\mathbf{p}_j^{(R)}$, where $j \in \{1, 2, 3\}$ and $R \in \{A, B\}$.

Since the constituent states $\rho_i^{(R)}$ are uncorrelated in the statistical mixture, the variances and covariances of the quadratures of these mixed states are given by:

$$\left\langle \left(\mathbf{X}_j^{(R)} \right)^2 \right\rangle = \frac{1}{n} \sum_{m=1}^n \left\langle \left(X_{3m-(3-j)}^{(R)} \right)^2 \right\rangle, \quad (\text{A2})$$

$$\frac{1}{2} \left\langle \left[\mathbf{X}_p^{(R)}, \mathbf{X}_q^{(S)} \right]_+ \right\rangle = \frac{1}{2n} \sum_{m=1}^n \left\langle \left[X_{3m-(3-p)}^{(R)}, X_{3m-(3-q)}^{(S)} \right]_+ \right\rangle, \quad (\text{A3})$$

where $R, S \in \{A, B\}$, $p = 2$, and $q \in \{1, 3\}$, $X_i^{(R)} \in \{x_i^{(R)}, p_i^{(R)}\}$, with $[\cdot]_+$ denoting the anti-commutator.

$$\frac{1}{2} \langle [\mathbf{X}_1^{(k)}, \mathbf{X}_3^{(l)}]_+ \rangle = \frac{1}{2n} \sum_{m=2}^n \langle [X_{3m-3}^{(k)}, X_{3m-2}^{(l)}]_+ \rangle \quad (\text{A4})$$

The covariance matrix of the six-mode graph state is then constructed from these variances and covariances. We arrange the quadrature operators in the following order:

$$\mathbf{X} = \left(x_1^{(A)}, p_1^{(A)}, x_1^{(B)}, p_1^{(B)}, x_2^{(A)}, p_2^{(A)}, x_2^{(B)}, p_2^{(B)}, x_3^{(A)}, p_3^{(A)}, x_3^{(B)}, p_3^{(B)} \right)^T. \quad (\text{A5})$$

With this ordering, the covariance matrix σ of the six-mode graph state is given by:

$$\sigma = \begin{pmatrix} \mathbf{V} & \mathbf{0} & \mathbf{C} & -\mathbf{C} & \frac{n-1}{n}\mathbf{C} & \frac{n-1}{n}\mathbf{C} \\ \mathbf{0} & \mathbf{V} & \mathbf{C} & -\mathbf{C} & -\frac{n-1}{n}\mathbf{C} & -\frac{n-1}{n}\mathbf{C} \\ \mathbf{C} & \mathbf{C} & \mathbf{V} & \mathbf{0} & \mathbf{C} & -\mathbf{C} \\ -\mathbf{C} & -\mathbf{C} & \mathbf{0} & \mathbf{V} & \mathbf{C} & -\mathbf{C} \\ \frac{n-1}{n}\mathbf{C} & -\frac{n-1}{n}\mathbf{C} & \mathbf{C} & \mathbf{C} & \mathbf{V} & \mathbf{0} \\ \frac{n-1}{n}\mathbf{C} & -\frac{n-1}{n}\mathbf{C} & -\mathbf{C} & -\mathbf{C} & \mathbf{0} & \mathbf{V} \end{pmatrix}. \quad (\text{A6})$$

Here, \mathbf{V} and \mathbf{C} are 2×2 matrices representing the variances and covariances of the quadrature operators, respectively. These can be expressed as a function related to the squeezed quadrature variance v and excess AS noise of the squeezed state employed in generating the dual rail cluster state Eq.17. Specifically, \mathbf{V} is the covariance matrix of a single mixed state, and \mathbf{C} captures the correlations between different mixed states.

The factor $\frac{n-1}{n}$ within the covariance matrix are due to the fact that the count of vertices in a group that includes the extreme vertices cannot match the number of edges linking them. this factor makes the multi partite Gaussian state impure. One can purify this impurity, introduced due to finite states, by introducing additional modes. Alternatively, one can consider pure six mode covariance matrix by removing the factor $\frac{n-1}{n}$. Introducing additional modes to purify the covariance matrix Eq.A6 would give us a tighter bound than considering the covariance matrix Eq.15 . that is, considering the pure six mode covariance matrix to estimate Holevo bound is more pessimistic than considering a purified state corresponding to covariance matrix Eq.A6, to estimate the Holevo bound. For sufficiently large n , the covariance matrix σ can be approximated to Eq.15 a pure six mode graph state and hence the improvement achieved through purification is insignificant.

Appendix B Congruence Transformation for Covariance Matrices

Given an original covariance matrix Σ of dimensions $12n \times 12n$, of the modes of the dual-rail cluster state under consideration for grouping, we can derive the covariance matrix σ of dimensions 12×12 corresponding to the six-mode graph state. This is achieved by applying a congruence transformation using a matrix \mathbf{A} of size $12 \times 12n$,

such that:

$$\boldsymbol{\sigma} = \frac{1}{n} \mathbf{A} \boldsymbol{\Sigma} \mathbf{A}^\top. \quad (\text{B7})$$

The ordering of quadratures in covariance matrix of the modes of dual rail cluster states considered for grouping is:

$$(x_1^{(a)}, p_1^{(a)}, x_1^{(b)}, p_1^{(b)}, x_2^{(a)}, p_2^{(a)}, x_2^{(b)}, p_2^{(b)}, \dots) \quad (\text{B8})$$

Here, \mathbf{A}^\top denotes the transpose of \mathbf{A} . This operation effectively projects the original covariance matrix onto a lower-dimensional subspace defined by \mathbf{A} , capturing the relevant quadrature correlations between the groups (color classes) of modes.

\mathbf{A} consists of vectors that indicate the modes present within a color class.

$$\mathbf{A}_{ij} = \begin{cases} 1 & \text{if } j \equiv i \pmod{11} \\ 0 & \text{otherwise} \end{cases} \quad (\text{B9})$$

A congruence transformation for the covariance matrix is possible provided the modes within each color class remain uncorrelated. However, if correlations exist among modes within a color class, the congruence transformation outlined above does not yield the covariance matrix of the statistical mixture defined by such coloring scheme.

$$\text{Note: } \mathbf{X}_{\text{six-mode}} \neq \frac{1}{\sqrt{n}} \mathbf{A} \mathbf{X}_{\text{dual}}$$

Based on the above congruence transformation, one might be inclined to define the quadrature operation of the six-mode graph state as a linear combination of the quadrature operators from the constituent states in the dual rail cluster state. However, it is essential to recognize that statistical mixtures cannot be represented by linear transformations of quadrature operators because the modes are not coherently combined. Instead, the covariance matrix of the mixture is the average of the covariance matrices of the constituent states.

B.1 Congruence transformation for adjacency matrices

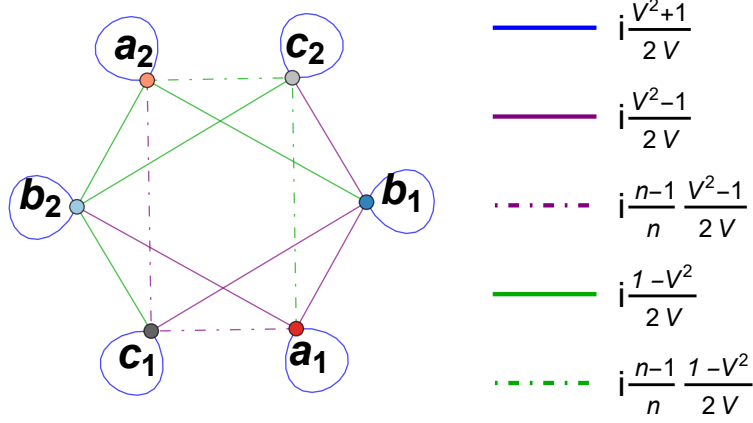
A complex-weighted adjacency matrix is used in continuous-variable quantum computing to represent Gaussian pure states, extending the real-weighted graphs of ideal cluster states to more realistic, physical states [31]. This formalism simplifies the analysis of entanglement structures, Gaussian operations, and deviations from ideal behaviors, which are essential for applications in CV quantum computing. Thus, we define a similar transformation to the one used in the previous section, enabling us to derive the adjacency matrix for a six-mode graph state $\mathbf{Z}_{\text{six-mode}}$ from the adjacency matrix of a dual-rail cluster state \mathbf{Z}_{dual} .

$$\mathbf{Z}_{\text{six-mode}} = \frac{1}{n} \mathbf{B} \mathbf{Z}_{\text{dual}} \mathbf{B}^\top \quad (\text{B10})$$

$$\mathbf{B}_{ij} = \begin{cases} 1 & \text{if } j \equiv i \pmod{5} \\ 0 & \text{otherwise} \end{cases} \quad (\text{B11})$$



(a) Complex weighted graph of dual rail cluster state



(b) Complex weighted graph of quotient graph derived from dual rail cluster state.

Fig. B1

Appendix C Parameter estimation

To estimate the channel transmission t , we use the fact that the correlation between the measurements of the dealer and the remote user scales as \sqrt{t} . Specifically, we can estimate the channel transmission from the following relation:

$$\sqrt{t} \mathcal{C} = \frac{1}{n} \sum_{i=1}^n d_i u_i := C_{du}, \quad (\text{C12})$$

where $\mathcal{C} = (1/2)\langle [X^d, X^u]_+ \rangle$ is the expectation value of the anticommutator of the quadrature operators X^d and X^u , measured by the dealer and the user before the state is sent through the channel. Here, d_i and u_i are the measurement outcomes corresponding to these quadratures for the dealer and the remote user, respectively.

We define C_{du} as:

$$C_{du} := \frac{1}{n} \sum_{i=1}^n d_i u_i, \quad (\text{C13})$$

which serves as an estimator for $\sqrt{t}\mathcal{C}$.

Rearranging the equation, we express the transmission t as:

$$t = \left(\frac{C_{du}}{\mathcal{C}} \right)^2. \quad (\text{C14})$$

Since C_{du} is a random variable due to measurement fluctuations, we are interested in the variance of our estimator for t :

$$\text{Var}[t] = \frac{\text{Var}[C_{du}^2]}{\mathcal{C}^4}. \quad (\text{C15})$$

Assuming that C_{du} is approximately normally distributed (by the Central Limit Theorem, since it is the average of n independent measurements), C_{du}^2 follows a non-central chi-squared distribution with one degree of freedom. The variance of C_{du}^2 is given by:

$$\text{Var}[C_{du}^2] = 2(\text{Var}[C_{du}])^2 + 4(\mathbb{E}[C_{du}])^2 \text{Var}[C_{du}]. \quad (\text{C16})$$

Since C_{du} is an average over n terms, its variance is:

$$\text{Var}[C_{du}] = \frac{1}{n} \text{Var}[X^d \tilde{X}^u], \quad (\text{C17})$$

where \tilde{X}^u is the quadrature operator of the state that the user possesses after transmission through the channel, and X^u is the quadrature operator of the state before it is sent through the channel.

Substituting back, we have:

$$\text{Var}[t] = \frac{2(\text{Var}[C_{du}])^2 + 4(\mathbb{E}[C_{du}])^2 \text{Var}[C_{du}]}{\mathcal{C}^4}. \quad (\text{C18})$$

For large n , the term $2(\text{Var}[C_{du}])^2$ is of order $1/n^2$ and can be neglected compared to $4(\mathbb{E}[C_{du}])^2 \text{Var}[C_{du}]$, which is of order $1/n$. Therefore, we approximate:

$$\text{Var}[t] \approx \frac{4(\mathbb{E}[C_{du}])^2 \text{Var}[C_{du}]}{\mathcal{C}^4}. \quad (\text{C19})$$

Substituting $\text{Var}[C_{du}] = \frac{1}{n} \text{Var}[X^d \tilde{X}^u]$ and $\mathbb{E}[C_{du}] = \mathbb{E}[X^d \tilde{X}^u]$, we obtain:

$$\text{Var}[t] \approx \frac{4(\mathbb{E}[X^d \tilde{X}^u])^2 \text{Var}[X^d \tilde{X}^u]}{n\mathcal{C}^4} = \frac{4t \text{Var}[X^d \tilde{X}^u]}{n\mathcal{C}^2}. \quad (\text{C20})$$

In [32], we have shown that combining measurement outcomes of both quadratures can increase the precision of our estimation of the channel transmission. Here, we apply the same principle by leveraging multiple correlations to decrease the variance of our estimators. For example, when the dealer has two modes that are correlated with the user's measurements, we can define the estimator:

$$\sqrt{t} \left(\frac{\mathcal{C}^a + \mathcal{C}^b}{2} \right) = \frac{1}{2n} \left(\sum_{i=1}^n d_i^a u_i + \sum_{i=1}^n d_i^b u_i \right) := C_{du}, \quad (\text{C21})$$

where $\mathcal{C}^i = \langle [X_i^d, X^u]_+ \rangle$ for $i = a, b$, and X_i^d are the quadratures of the modes possessed by the dealer.

For a symmetric case where $\mathcal{C}^a = \mathcal{C}^b$ and $\text{Var}[X_a^d \tilde{X}^u] = \text{Var}[X_b^d \tilde{X}^u]$, the new variance of the estimator for t becomes:

$$\text{Var}[t] \approx \frac{4t \text{Var}[X^d \tilde{X}^u]}{2n\mathcal{C}^2}. \quad (\text{C22})$$

We can generalize this result for any number k of symmetric correlations used to estimate the channel transmission:

$$\text{Var}[t] \approx \frac{4t \text{Var}[X^d \tilde{X}^u]}{kn\mathcal{C}^2}. \quad (\text{C23})$$

Thus, by leveraging multiple correlated modes, we reduce the variance of the estimator for the transmission t by a factor of k , enhancing the precision of our estimation.

We estimate the excess noise as follows.

$$V_\epsilon = \frac{1}{n} \sum_i^n u_i^2 + t(1 - \text{Var}[X^u]) - 1 \quad (\text{C24})$$

The variance of the excess noise estimator can be approximated to.

$$\text{Var}[V_\epsilon] \approx \frac{2}{n} (\text{Var}[\tilde{X}^u])^2 + \text{Var}[t](1 - \text{Var}[X^u])^2 \quad (\text{C25})$$

We now define the quadrature operators x_d and x_u for the three multipartite states under consideration. Recall that the tilde notation \tilde{x}_u has been introduced earlier to represent sending a mode with quadrature x_u through a channel with transmission t , specifically $\tilde{x}_u = \sqrt{t}x_u + \sqrt{1-t}x_0$, where x_0 is the quadrature operator of a vacuum state.

In protocols involving a six-mode graph state, the quadrature of each mode is a linear function composed of quadratures from four squeezed states. Any two modes have two of these squeezed states quadrature in common. Consequently, any two correlated modes of a six-mode graph state can be expressed in terms of the quadrature operators of six squeezed states, all characterized by the same quadrature variance. for example consider the following two quadratures corresponding to deal's mode x_d and mode meant for a remote user x_u :

$$x_d = \frac{1}{2}(p^{(2)} + p^{(4)} - x^{(1)} + x^{(3)}), \quad (\text{C26})$$

$$x_u = \frac{1}{2}(\mp p^{(4)} + p^{(6)} \pm x^{(3)} + x^{(5)}). \quad (\text{C27})$$

Here, $x^{(i)}$ denotes a squeezed quadrature with variance v , while $p^{(i)}$ denotes the corresponding anti-squeezed quadrature with variance $dv + \frac{1}{v}$.

Since we are dealing with Gaussian states, straightforward algebraic manipulations yield the following expression for the variance $\text{Var}[x_d \tilde{x}_u]$:

$$\text{Var}[x_d \tilde{x}_u] = \frac{t}{16} \left(5 \left(dv + \frac{1}{v} \right)^2 + 5v^2 + 6 \left(dv + \frac{1}{v} \right) v \right) + (1-t) \left(\frac{1+v(dv+v)}{2v} \right). \quad (\text{C28})$$

Turning to the three-mode GHZ state, the relevant quadratures are given by:

$$x_1 = \frac{\sqrt{2} p^{(1)} + x^{(2)} + \sqrt{3} x^{(3)}}{\sqrt{6}}, \quad x_2 = \frac{\sqrt{2} x^{(2)} - p^{(1)}}{\sqrt{3}}, \quad x_3 = \frac{-\sqrt{2} p^{(1)} - x^{(2)} + \sqrt{3} x^{(3)}}{\sqrt{6}}. \quad (\text{C29})$$

Although two of these modes incorporate quadrature components from three squeezed states each, and one mode has components from only two squeezed states, this difference does not influence the choice of which mode is sent through the transmission channel. The variance $\text{Var}[x_d \tilde{x}_u]$ remains the same, given by:

$$\text{Var}[x_d \tilde{x}_u] = \frac{t}{9} \left(2 \left(dv + \frac{1}{v} \right)^2 + 5v^2 + 2 \left(dv + \frac{1}{v} \right) v \right) + (1-t) \left(\frac{1+v(dv+2v)}{3v} \right). \quad (\text{C30})$$

For a DAN with a two-mode squeezed vacuum, the relevant quadratures for the dealer and the remote user modes are:

$$x_d = \frac{x^{(1)} + p^{(2)}}{\sqrt{2}}, \quad x_u = \frac{1}{2}(\sqrt{2} p_0 - x^{(1)} + p^{(2)}). \quad (\text{C31})$$

Similarly, we obtain:

$$\text{Var}[x_d \tilde{x}_u] = \frac{t}{8} \left(dv + \frac{1}{v} \right) \left(dv + \frac{1}{v} + 1 \right) + v(1+v) + (1-t) \left(\frac{1+v(dv+v)}{2v} \right). \quad (\text{C32})$$

References

- [1] Wang, J., Xu, G.-B., Jiang, D.-H.: Quantum voting scheme with greenberger-horne-zeilinger states. *International Journal of Theoretical Physics* **59**, 2599–2605 (2020) <https://doi.org/10.1007/s10773-020-04529-7>
- [2] Guo, Y., Feng, Y., Zeng, G.: Quantum anonymous voting with unweighted continuous-variable graph states. *Quantum Information Processing* **15**, 3327–3345 (2016) <https://doi.org/10.1007/s11128-016-1349-1>
- [3] Wang, Q., Yu, C., Gao, F., Qi, H., Wen, Q.: Self-tallying quantum anonymous voting. *Phys. Rev. A* **94**, 022333 (2016) <https://doi.org/10.1103/PhysRevA.94.022333>

- [4] Lau, H.-K., Weedbrook, C.: Quantum secret sharing with continuous-variable cluster states. *Phys. Rev. A* **88**, 042313 (2013) <https://doi.org/10.1103/PhysRevA.88.042313>
- [5] Wu, Y., Cai, R., He, G., *et al.*: Quantum secret sharing with continuous variable graph state. *Quantum Information Processing* **13**(5), 1085–1102 (2014) <https://doi.org/10.1007/s11128-013-0713-7>
- [6] Karlsson, A., Koashi, M., Imoto, N.: Quantum entanglement for secret sharing and secret splitting. *Phys. Rev. A* **59**, 162–168 (1999) <https://doi.org/10.1103/PhysRevA.59.162>
- [7] Pan, D., Long, G.-L., Yin, L., Sheng, Y.-B., Ruan, D., Ng, S.X., Lu, J., Hanzo, L.: *The Evolution of Quantum Secure Direct Communication: On the Road to the Qinternet* (2023)
- [8] Wang, C., Deng, F.G., Long, G.L.: Multi-step quantum secure direct communication using multi-particle green–horne–zeilinger state. *Optics Communications* **253**(1-3), 15–20 (2005) <https://doi.org/10.1016/j.optcom.2005.04.048>
- [9] Murta, G., Grasselli, F., Kampermann, H., Bruß, D.: Quantum conference key agreement: A review. *Advanced Quantum Technologies* **3**(11), 2000025 (2020) <https://doi.org/10.1002/qute.202000025>
- [10] Zhao, W., Shi, R., Feng, Y., Ruan, X.: Conference key agreement based on continuous-variable quantum key distribution. *Laser Physics Letters* **18**(7), 075205 (2021) <https://doi.org/10.1088/1612-202X/ac0915>
- [11] Menicucci, N.C., Loock, P., Gu, M., Weedbrook, C., Ralph, T.C., Nielsen, M.A.: Universal quantum computation with continuous-variable cluster states. *Physical Review Letters* **97**(11), 110501 (2006) <https://doi.org/10.1103/PhysRevLett.97.110501>
- [12] Menicucci, N.C.: Fault-tolerant measurement-based quantum computing with continuous-variable cluster states. *Physical Review Letters* **112**(12), 120504 (2014) <https://doi.org/10.1103/PhysRevLett.112.120504>
- [13] Larsen, M.V., Chamberland, C., Noh, K., Neergaard-Nielsen, J.S., Andersen, U.L.: Fault-tolerant continuous-variable measurement-based quantum computation architecture. *PRX Quantum* **2**(3), 030325 (2021) <https://doi.org/10.1103/PRXQuantum.2.030325>
- [14] Menicucci, N.C., Ma, X., Ralph, T.C.: Arbitrarily large continuous-variable cluster states from a single quantum nondemolition gate. *Phys. Rev. Lett.* **104**, 250503 (2010) <https://doi.org/10.1103/PhysRevLett.104.250503>
- [15] Menicucci, N.C.: Temporal-mode continuous-variable cluster states using linear

- optics. Phys. Rev. A **83**, 062314 (2011) <https://doi.org/10.1103/PhysRevA.83.062314>
- [16] Yokoyama, S., Ukai, R., Armstrong, S., *et al.*: Ultra-large-scale continuous-variable cluster states multiplexed in the time domain. Nature Photonics **7**, 982–986 (2013) <https://doi.org/10.1038/nphoton.2013.287>
- [17] Larsen, M.V., *al.*: Deterministic generation of a two-dimensional cluster state. Science **366**, 369–372 (2019) <https://doi.org/10.1126/science.aay4354>
- [18] Menicucci, N.C., Flammia, S.T., Zaidi, H., Pfister, O.: Ultracompact generation of continuous-variable cluster states. Phys. Rev. A **76**, 010302 (2007) <https://doi.org/10.1103/PhysRevA.76.010302>
- [19] Menicucci, N.C., Flammia, S.T., Pfister, O.: One-way quantum computing in the optical frequency comb. Phys. Rev. Lett. **101**, 130501 (2008) <https://doi.org/10.1103/PhysRevLett.101.130501>
- [20] Chen, M., Menicucci, N.C., Pfister, O.: Experimental realization of multipartite entanglement of 60 modes of a quantum optical frequency comb. Phys. Rev. Lett. **112**, 120505 (2014) <https://doi.org/10.1103/PhysRevLett.112.120505>
- [21] Roslund, J., Araújo, R., Jiang, S., *et al.*: Wavelength-multiplexed quantum networks with ultrafast frequency combs. Nature Photonics **8**, 109–112 (2014) <https://doi.org/10.1038/nphoton.2013.340>
- [22] Pickston, A., Ho, J., Ulibarrena, A., *et al.*: Conference key agreement in a quantum network. npj Quantum Information **9**, 82 (2023) <https://doi.org/10.1038/s41534-023-00750-4>
- [23] Adesso, G., Serafini, A., Illuminati, F.: Multipartite entanglement in three-mode gaussian states of continuous-variable systems: Quantification, sharing structure, and decoherence. Phys. Rev. A **73**, 032345 (2006) <https://doi.org/10.1103/PhysRevA.73.032345>
- [24] Hsieh, H.-Y., Chen, Y.-R., Wu, H.-C., Chen, H., Ning, J., Huang, Y.-C., Wu, C.-M., Lee, R.-K.: Extract the degradation information in squeezed states with machine learning. Physical Review Letters **128**(7), 073604 (2022) <https://doi.org/10.1103/PhysRevLett.128.073604>
- [25] Nielsen, M.A., Chuang, I.L.: Quantum Computation and Quantum Information, 10th anniversary edition edn. Cambridge University Press, ??? (2010)
- [26] Weedbrook, C., Pirandola, S., García-Patrón, R., Cerf, N.J., Ralph, T.C., Shapiro, J.H., Lloyd, S.: Gaussian quantum information. Rev. Mod. Phys. **84**, 621–669 (2012) <https://doi.org/10.1103/RevModPhys.84.621>

- [27] Leverrier, A.: Composable security proof for continuous-variable quantum key distribution with coherent states. *Phys. Rev. Lett.* **114**, 070501 (2015) <https://doi.org/10.1103/PhysRevLett.114.070501>
- [28] Leverrier, A., Grosshans, F., Grangier, P.: Finite-size analysis of a continuous-variable quantum key distribution. *Phys. Rev. A* **81**, 062343 (2010) <https://doi.org/10.1103/PhysRevA.81.062343>
- [29] Adesso, G., Serafini, A., Illuminati, F.: Multipartite entanglement in three-mode gaussian states of continuous-variable systems: Quantification, sharing structure, and decoherence. *Phys. Rev. A* **73**, 032345 (2006) <https://doi.org/10.1103/PhysRevA.73.032345>
- [30] Loock, P., Braunstein, S.L.: Multipartite entanglement for continuous variables: A quantum teleportation network. *Phys. Rev. Lett.* **84**, 3482–3485 (2000) <https://doi.org/10.1103/PhysRevLett.84.3482>
- [31] Menicucci, N.C., Flammia, S.T., Loock, P.: Graphical calculus for gaussian pure states. *Phys. Rev. A* **83**, 042335 (2011) <https://doi.org/10.1103/PhysRevA.83.042335>
- [32] Oruganti, A., Derkach, I., Usenko, V.C.: Continuous-variable quantum key distribution with noisy squeezed states (2024). <https://arxiv.org/abs/2404.05247>